HHS Public Access

Author manuscript

*Magn Reson Med*. Author manuscript; available in PMC 2016 December 01.

Published in final edited form as:

*Magn Reson Med*. 2015 December ; 74(6): 1556–1563. doi:10.1002/mrm.25995.

# Dynamic Glucose Enhanced (DGE) MRI for Combined Imaging of Blood Brain Barrier Break Down and Increased Blood Volume in Brain Cancer

**Xiang Xu**[1,2,#], **Kannie WY Chan**[1,2,#,*], **Linda Knutsson**[3], **Dmitri Artemov**[1,4], **Jiadi Xu**[1,2], **Guanshu Liu**[1,2], **Yoshinori Kato**[1,4,5], **Bachchu Lal**[6], **John Laterra**[6], **Michael T. McMahon**[1,2], and **Peter C.M. van Zijl**[1,2,*]

[1]Russell H. Morgan Department of Radiology and Radiological Science, The Johns Hopkins University School of Medicine, Baltimore, MD, United States

[2]F.M. Kirby Research Center for Functional Brain Imaging, Kennedy Krieger Institute, Baltimore, MD, United States

[3]Department of Medical Radiation Physics, Lund University, Lund, Sweden

[4]Division of Cancer Imaging Research and JHU In Vivo Cellular Molecular Imaging Center, The Johns Hopkins University School of Medicine, Baltimore, MD, United States

[5]Life Science Tokyo Advanced Research Center, Hoshi University School of Pharmacy and Pharmaceutical Sciences, Tokyo, Japan

[6]Department of Neurology, Oncology, and Neuroscience, The Johns Hopkins Medicine, and The Hugo W. Moser Research Institute at Kennedy Krieger, Baltimore, MD, United States

## Abstract

**Purpose—**Recently, natural D-glucose was suggested as a potential biodegradable contrast agent. The feasibility of using D-glucose for dynamic perfusion imaging was explored to detect malignant brain tumors based on blood brain barrier breakdown.

**Methods—**Mice were inoculated orthotopically with human U87-EGFRvIII glioma cells. Time-resolved glucose signal changes were detected using chemical exchange saturation transfer (glucoCEST) MRI. Dynamic glucose enhanced (DGE) MRI was used to measure tissue response to an intravenous bolus of D-glucose.

**Results—**DGE images of mouse brains bearing human glioma showed two times higher and persistent changes in tumor compared to contralateral brain. Area-under-curve (AUC) analysis of DGE delineated blood vessels and tumor and had contrast comparable to the AUC determined using dynamic contrast enhanced (DCE) MRI with GdDTPA, both showing a significantly higher AUC in tumor than in brain ($p<0.005$). Both CEST and relaxation effects contribute to the signal change.

*To whom correspondence may be addressed: pvanzijl@mri.jhu.edu; kanniec@mri.jhu.edu.
#Both authors contributed equally

**Conclusion—**DGE MRI is a feasible technique for studying brain tumor enhancement reflecting differences in tumor blood volume and permeability with respect to normal brain. We expect DGE will provide a low-risk and less expensive alternative to DCE MRI for imaging cancer in vulnerable populations, such as children and patients with renal impairment.

### Keywords

Dynamic glucose enhanced MRI; D-glucose; brain cancer; chemical exchange saturation transfer (CEST)

## Introduction

Imaging plays a crucial role in the diagnosis and therapeutic monitoring of cancer. Contrast agents provide increased sensitivity or specificity for visualizing anatomy and physiology that is often not attainable with non-contrast imaging. For instance, the use of contrast agents is a powerful tool to assess different aspects of the tumor microenvironment, such as active tissue metabolism with PET/SPECT and tissue-perfusion related parameters (blood flow, blood volume and blood brain barrier permeability) with dynamic contrast enhanced CT (DCE-CT) or MRI (DCE-MRI) (1). In the clinic, tumor blood volume and permeability can be assessed using DCE-CT (2) or DCE-MRI (3). The principle is to inject a bolus of contrast agent intravenously and measure signal change as a function of time using rapid sequential imaging. Due to angiogenesis and disruption of the blood-brain-barrier (BBB), aggressive tumors are enhanced compared to normal tissue and display a higher blood volume and increased permeability.

While very safe overall, current clinical contrast agents contain synthetic iodine (CT) or paramagnetic (MRI) labels that have potential side effects, especially in patients with impaired renal function. Recent studies show long-term retention of gadolinium in the brain (4). CT uses radioactivity for detection, making it difficult to use repeatedly (e.g. for treatment monitoring), especially in children. Thus, there is a need to exploit low risk biocompatible contrast agents for tumor diagnosis.

D-glucose is a natural compound that is FDA-approved for non-imaging purposes. Recently, it has shown potential as an MRI contrast agent that can be detected using chemical exchange saturation transfer (CEST) (5,6). Each glucose molecule contains five hydroxyl protons that exchange with bulk water protons. Their saturation affects the water MRI signal, thus allowing detection of the presence of glucose. Since the exchange rate is very fast, k ~ 500 –10,000 Hz depending on pH (7), and five OH groups are present per molecule, a large sensitivity gain can be achieved (8) pushing the detection limit as low as a few millimolar. CEST properties of hydroxyl protons have been studied in glucose and glycogen (9), glucosaminoglycan (GAG) (10,11) and small peptides (12). We and others have recently shown the detection of D-glucose or its derivatives *in vivo* with CEST (5,6,13–15), chemical exchange sensitive spin lock (CESL) (16,17) or chemical exchange based T2 relaxation enhancement (18,19).

While the use of D-glucose is generally associated with metabolic studies, the aim of the present study is to examine the feasibility of performing dynamic glucose enhanced (DGE)

imaging to assess increases in blood volume and BBB breakdown in a brain tumor model and compare it to conventional dynamic contrast enhanced (DCE) MRI using gadolinium.

## Methods

Animal experiments were approved by the Johns Hopkins University Institutional Animal Care and Use Committee.

### Implantation of human cancer cells in mice

Human U87-EGFRvIII cells were grown in Dulbecco's Modified Essential Medium high glucose with L-glutamine and sodium pyruvate (Mediatech Inc.) supplemented with 10% fetal bovine serum, 1% of 10 mM MEM-non-essential amino acids and penicillin-streptomycin (20). Severe combined immune deficiency (SCID) mice (female; 6–8 weeks; NCI, Frederick, MD) were anesthetized with isoflurane. Cells ($1\times10^5$ cells/2 μl; at 0.5 μl/min) were implanted orthotopically by stereotaxic injection into the right caudate/putamen. Seven mice were imaged either on day 6, 7 or 8 post-implantation. However, we noticed that when tumors became bigger and heterogeneous, they took up a lot of water during glucose injection, as indicated by narrowing of the Z-spectra. This happened in two mice for which the data were acquired on day 8 post-inoculation. These mice were therefore not included in the dynamic analysis.

### Injection and imaging protocols

All MRI images were acquired on a horizontal bore 11.7T Bruker Biospec system equipped with a 23 mm volume transceiver coil. Mice fasted overnight with water access were anesthetized by isoflurane, and kept warm with a heating bed. The tail vein was cannulated with a catheter and the dead volume minimized to 30 μL. A connector with 4 lines was connected to a 2.8 M D-glucose solution (0.5 g/mL, clinical-grade Dextrose, Hospira), Gd-DTPA solution (Magnevist®; 100 mM in saline), heparinized saline, and the tail vein. All lines were controlled by two-way stopcocks with 1-mL syringes, and only one line was open at a time. D-glucose injection was done with a syringe pump.

Anatomical images were acquired to identify the slice with maximum tumor size. DGE images were collected by saturating at the hydroxyl proton frequency offset of 1.2 ppm at a temporal resolution of 10 s. Detection was done using a Rapid Acquisition with Relaxation Enhancement (RARE) sequence, TR/TE=5.0 s/3.8 ms, RARE factor 23, partial Fourier acceleration factor of 1.4. A single slice with $0.125\times0.250$ mm$^2$ in plane resolution and thickness 1 mm was imaged (FOV 1.6 cm$^2$). Saturation was achieved by a single magnetization transfer (MT) pre-pulse (3s, $B_1$=1.6 μT). An image with the same sequence timing but no saturation pulse was acquired ($S_0$ image) prior to injection. The dynamic scanning started before glucose injection by acquiring 18 baseline scans over 3 min. Without stopping the scanning, a bolus of 0.15 mL D-glucose was infused over a 1 min period. The dynamic acquisition continued for a total of 15 min. CEST Z-spectra were acquired over a frequency range from −5.2 to 5.2 ppm (0.4 ppm intervals) before and after dynamic acquisition. The experimental scheme is shown in Fig. 1. Gd-DCE images were acquired one hour post glucose injection. Multi-slice T1-weighted images were obtained using a non-

selective saturation-recovery gradient echo with TE/TR/FA =1.5 ms/26 ms/90° (21), at the same spatial and temporal resolution as DGE imaging. A large flip angle was used to increase T1 weighting and reduce the effect of water exchange as recommended in the literature (21,22)). After acquiring 8 pre-contrast images, a bolus injection (10s) of 0.1 mL of 0.1 M Gd-DTPA was given and 32 post-contrast images were collected over 320 s.

### Data analysis

For the DGE data, the first four images were discarded and the image intensity (S) of the others was normalized by dividing with $S_0$. Baseline images were generated for both DGE and DCE by averaging the eight pre-injection images ($S_{base}$). DCE images were normalized to $S_{base}$. Glucose and Gd dynamic difference images were generated by taking the difference between each dynamic image and the average of 14 or 8 pre-injection images, respectively. Average dynamic time curves were smoothed by applying a low-pass filter to reduce the motion artifacts. However, one mouse was excluded due to excessive motion artifacts. For both DGE and DCE MRI data, the semi-quantitative parameter area-under-curve (AUC) was calculated using:

$$AUC=\Sigma_1^n \frac{S_{base}}{S_0 or S_{base}} - \frac{S(t_n)}{S_0 or S_{base}} = \Sigma_1^n \frac{\Delta S(t_n)}{S_0 or S_{base}} \quad [1]$$

in which n=30, corresponding to 300 s after glucose/Gd injection.

The student's t-test was used to compare tumor and contralateral brain. The signal to noise ratio (SNR) was calculated as:

$$SNR(t)=\frac{S(t)_{tumor,or\ brain}}{\sqrt{2}SD(S_1 - S_2)} \quad [2]$$

in which the standard deviation (SD) is a measure of variation in noise over two consecutive acquisitions, $S_1$ and $S_2$ prior to injection. The contrast to noise ratio (CNR) was calculated by

$$CNR(t)=SNR(t)_{tumor} - SNR(t)_{brain} \quad [3]$$

## Results

Figure 2a shows the DGE difference images at 1.2 ppm of a typical mouse before, during and after glucose injection. Prior to injection, negligible contrast change is observed in the brain and the surrounding tissues. When injection starts, the arterial vessels in and around the brain show enhancement immediately. Subsequently, the tumor contrast starts to increase as compared to contralateral brain. The enhancement persists during the course of the bolus. Figure 2b shows the dynamic curves for regions of interest (ROIs) drawn around the tumor and corresponding contralateral brain. Tumor consistently shows a higher percentage change in signal than contralateral brain, both immediately following injection and for a prolonged period post-injection.

Figure 3a shows the average DGE curves (n=4) for tumor and contralateral brain. An elevated uptake of glucose is clear in the tumor, showing $\Delta S/S_0$=1.5–3% at the maximal tumor enhancement (10 s post injection completion) and about 1% at 300 s post-injection (Fig. 3a). For contralateral brain this was about 0.5–1.5% at maximum and 0.3% or less at 300s (Fig. 3b). The tumor enhancement was about twice that of contralateral brain at the maximum, namely 1.90±0.47% and 0.98±0.42% ($p$=0.029), respectively. In contralateral brain, the increase of signal happened during the injection after which it decreased back to indistinguishable from baseline in 2–3 minutes. In contrast, the elevated uptake of glucose in the tumor area persisted, at least up to 12 min post-injection, with an average $\Delta S/S_0$ in water signal of ~0.7% higher than baseline, corresponding to about 0.8 molar signal strength. Notice that the DGE signal intensity ($S/S_0$) is in units of percent and that a $\Delta S/S_0$ of 1% corresponds to a 2.5% relative change in $S_{base}/S_0$, which was 41% for our saturation parameters. One of the mice showed a sharp decrease in signal 300 s post injection in both the tumor and the contralateral region. The exact reason is not known, but a possible explanation is a rapid insulin response in this mouse. In DCE (Fig. 3d), the tumor dynamic curve showed a continuous increase after injection. At 300 s post-injection (Fig. 3e), the signal change in the tumor was significantly (p=0.006) higher than in contralateral brain.

Representative anatomical, DGE, and DCE images (overlaid on an anatomical image) at 300 s post-injection are shown in Fig. 4. The mean CNR (n=4) values were 3.23±1.84 and 1.27±0.53 for DGE and DCE, respectively, which allowed clear delineation of the tumor. Some signal enhancement is visible in the lateral ventricles, which we attribute to glucose uptake and volumetric change in the ventricles (23). AUC images were calculated to study uptake and retention of glucose (Fig. 5). Both DGE-AUC and DCE-AUC images show a hyperintense tumor region, allowing a robust separation of tumor and brain. A slight difference visible in the center of the tumor in the DGE and DCE AUC images could be due to the difference in SNR. While the gadolinium AUC has negligible enhancement outside the tumor, the glucose AUC shows some brain enhancement as expected based on tissue glucose transport (see Discussion). Figs 5c and 5d show the mean AUC for tumor and contralateral brain for both methods, showing significant differences ($p < 0.005$, n=4) between the tumor and the brain.

In Figure 6, Z-spectra acquired before and after the dynamic scan period are shown. These provide information about the origin of the tail in the DGE tumor curve of Fig 3a. Interestingly, The width of Z-spectra show a significant ($p < 0.05$) broadening for the tumor (Fig 6a) and negligible difference for contralateral brain (Fig 6b) while no difference is visible in the $MTR_{asym}$ spectra (Fig. 6c) for either of these.

## Discussion

The results show that it is possible to perform dynamic MRI studies for the enhanced detection of malignant brain tumors using natural D-glucose as a contrast agent. Normal brain also shows a small enhancement immediately after injection, however, contrary to tumor, enhancement was negligible at 300 s post-injection. The longer retention in tumor can be ascribed to the well-known effect of poor drainage resulting from abnormal vasculature. Contrary to DGE, the DCE curves (Fig. 3d) showed an initial signal decrease

directly after injection due to shortening of T2* due to a transient high concentration of Gd. This was followed by a gradual increase in the signal difference $\Delta S/S_0$, attributed to the contrast agent leaking out into the EES and a dominant shortening of T1.

From the uptake curves of DGE and DCE it appears that D-glucose enters the EES immediately, while Gd enters more slowly. We attribute this to the smaller size of D-glucose and these initial data may indicate a possible increased sensitivity of D-glucose for the detection of BBB breakdown. When comparing the two dynamic enhancement techniques it is important to consider the difference between D-glucose and gadolinium. Most Gd-based MR contrast agents used in perfusion studies remain intravascular (in plasma) in healthy brain. In tumor, due to partial breakdown of blood-brain-barrier (BBB), the Gd-based agent is confined to plasma and extravascular extracellular space (EES). D-glucose, on the other hand, not only diffuses through the leaky BBB of tumors, but also is actively transported across the BBB and thus enters cells in tumors as well as in healthy brain (24), as reflected in Figs 2a, 4b, 5a. This facilitated transport may be an additional contributor to improved detection of BBB breakdown. Upon entering the tumor cells one can assume instantaneous disappearance of glucose CEST signal, due to rapid phosphorylation and glycolytic conversion. Glycolytic intermediates with OH groups, such as glucose-6-phosphate, fructose-6-phosphate, and fructose-1,6-bisphosphate, can be detected by CEST in millimolar concentration. However, the cellular equilibrium concentrations of these metabolites are extremely low (< 0.2 mM) (25) in the tumor since they are rapidly converted to lactate. Therefore, these metabolites do not have a sufficient CEST signal for detection, resulting in a negligible the intracellular CEST signal. In normal brain, phosphorylated glucose intermediates have also been reported to be of very low concentration (~80 μM glucose-6-phosphate, ~14 μM fructose-6-phosphate, and ~30 μM fructose-1,6-bisphosphate) (26–29) before they are further metabolized in the TCA cycle (30,31). Based on this, it is a reasonable assumption that the observed signals mainly originate from the EES and the plasma.

To quantify the uptake and retention, AUC images were calculated. The DGE-AUC images (Fig. 5a) showed strong significant contrast between tumor and contralateral brain. The areas of enhancement in DGE- and DCE-AUC images were similar indicating that the two methods reflect comparable properties for this particular tumor type. The DCE-AUC relates to the blood volume, permeability of the vascular endothelium, and the fraction of EES accessed but it is not a quantitative measure of perfusion. In DCE, the extended Tofts model is commonly used to describe the equilibrium of Gd tracer between the EES and the plasma (32,33). However, for the comparison of DCE and DGE we limited ourselves to AUC assessment because the determination of the kinetic parameters in DGE is more complicated and challenging. First, the cellular glucose uptake and consumption has to be included and equations developed. (28,34,35). When interpreting the time-dependent glucose signal, the initial part is expected to reflect mainly tissue perfusion-related properties, such as blood volume, extravascular and extracellular space (EES) volume and BBB permeability. However, depending on the rate of glucose transport into the tumor cell (rate limiting step), the later time points contributing should also include the effect of glucose metabolized by the tumor and tissue, similar to models used for glucose metabolism in tumors (25) and tissue (28, 34) published for $^{13}$C-glucose metabolic studies, where the metabolic products as

well as the D-glucose substrate have been measured. A second issue for an accurate determination of perfusion-related parameters is the linearity of the measured signal changes with glucose concentration. While the glucose concentration is sufficiently low to warrant linearity of the CEST signal (9), D-glucose also reduces the water T2 relaxation through exchange (18,19), broadening the direct water saturation curve, in a manner synergistic with glucoCEST increases. This broadening effect can be seen in the Z-spectra acquired prior and post injection in the tumor region. Third, the injection over a period of about one minute appears to be too slow to separate the initial kinetics for glucose uptake in the tumor and brain tissue, which peaked simultaneously. A more complex model needs to be established to take into account for all these contributions before determining kinetic parameters, especially glucose metabolism.

Previous studies have reported glucoCEST imaging with a continuous glucose infusion up to 20 min (5,13) using Z-spectra based asymmetry analysis to measure CEST-based signal changes (36). Such an analysis is very sensitive to $B_0$-inhomogeneity and interfering saturation transfer effects that are also asymmetric with respect to the water frequency (37,38). In our DGE study, it was not necessary to reference another frequency, because OH protons exchange very fast ($k > 10^3$ Hz). The resulting OH resonance spans over a few ppm making measurement of its change insensitive to $B_0$ inhomogeneity. We therefore collected our DGE images at a single frequency of 1.2 ppm, which allowed us to detect transient dynamic changes immediately after injection. In order to get some insight into the mechanism of contrast, we acquired Z-spectra before and after the dynamic phase of the study. In line with the dynamic study, we found a difference in the Z-spectra in the tumor and not in contralateral brain (Fig. 6). Surprisingly, however, the $MTR_{asym}$ spectra showed negligible difference in both tumor and brain, indicating that the remaining longer-term difference was due only to broadening of the Z-spectrum and not due to a CEST based effect. In earlier work, acquiring Z-spectra during prolonged infusion, a clear glucoCEST spectral difference was found (5,6) We intend to investigate the relative contributions of relaxation and glucoCEST during and post-infusion in the future.

An important consideration is the potential to translate the DGE technology to humans. D-glucose is expected to be safe for patients with limited kidney function, but may be an issue for diabetic patients. With respect to dose, a proper comparison of human to animals requires a body surface area (BSA) conversion (39), in which the mouse dose per body weight should be about 12 times higher than human. In our study we injected 0.15 mL of 50% dextrose, which would be equivalent to a 50 mL vial of 50% dextrose in a human of 60 kg consistent with the dose used in a glucose tolerance test (40). Other requirements are MRI signal sensitivity and selectivity of the changes related to D-glucose. The signal sensitivity of glucoCEST signal changes is related mainly to the exchange rate and number of OH groups and, as such, not field dependent. The selective excitation of the OH group is an issue both at 11.7T and 3T because the resonance is very broad (determined by the exchange rate). Since we measure dynamic signal changes upon injection of glucose while saturating in the center of the OH frequency region, it is logical to assume that we measure the changes based on glucose. We have started to translate the DGE technique to humans at 7T (41) and found no SAR issue, similar to other CEST and magnetization transfer studies on human systems. At 3T, the detection of protons that exchange fast and resonate close to

water is challenging. However, the data in this and previous papers show that the signal is a combined effect from CEST and relaxation broadening. Together with other advantages at 3T such as improved $B_0$ and $B_1$ field, we predict the DGE technique is possible. Also, even though the sensitivity of DCE may be better than DGE, DGE may provide additional information due to the different biodistributions between Gd-based contrast agents and D-glucose. An alternative MRI method to assess tumor perfusion is arterial spin-labeling (ASL) (42). While ASL has a permeability component (43), this generally is neglected in the modeling (fast exchange assumed).

Finally, there has been a misconception that glucoCEST will be hard to translate to humans because it should suffer from the same problem as FDG PET in that it will be difficult to separate out normal gray matter from tumor signals. This is not the case and to comprehend this, it is important to realize that the observed signals are very different in PET versus glucoCEST, namely metabolic activity in terms of metabolized (phosphorylated) glucose trapped in the cell by FDG-PET, versus glucose substrate in plasma and tissue by dynamic glucoCEST. PET experiments are geared to measuring close to the highest concentration of trapped phosphorylated FDG (6-P-FDG) built up by metabolism and counteracted by radioactive decay, which is why measurements are done about 60 minutes post-injection of radioactively labeled FDG, when most of the non-phosphorylated tracer is cleared. In glucoCEST we exploit several facts: a) transport of glucose is facilitated and, in normal brain, the concentration in plasma is about four times higher than that in tissue and also about four times higher in interstitium than in the cell (34,44). b) As mentioned, the concentrations of 6-phosphorylated glucose and intermediate metabolic products in the cell in normal brain are in the low micromolar concentration range (28). Thus, these compounds have negligible contribution to the glucoCEST signal. Moreover, pyruvate and lactate are not visible in glucoCEST and the metabolic product in normal brain (glutamate) is hard to detect at the $B_1$ value used. While the CEST effect of these metabolites is expected to be minimal, further experiments are needed to confirm this. c) In high-grade tumors there is instantaneous disappearance of glucoCEST signal upon cell entry due to rapid phosphorylation and glycolytic conversion to lactate (25). Therefore, extracellular glucose substrate is the predominant compound measured in DGE-MRI. Thus, while FDG-PET cannot separate brain and tumor uptake very well due to the ending of metabolism after phosphorylation and a consequential high concentration of 6-P-FDG in gray matter as well as tumor, we can easily accomplish tumor-brain specificity with glucoCEST. Notice that, as a consequence of measuring metabolism versus perfusion, FDG-PET and glucoCEST are complimentary methods and can be used simultaneously in the future in MR-PET scanners.

## Conclusions

We demonstrated the possibility of using natural biodegradable D-glucose for dynamically enhancing human brain tumors in an experimental orthotopic mouse model. DGE and DCE area-under-curve images showed similar areas of enhancement, indicating both methods measure effects related to angiogenesis and BBB breakdown in the tumors. These first results confirm the potential for using D-glucose as a diagnostic agent for MRI, and of DGE for assessing changes in blood volume and permeability. D-glucose is already FDA approved as a drug for human studies for non-imaging purposes (glucose tolerance testing) (40) and

translation to the clinic for the indication as a contrast agent is expected to be fast as basic safety testing has already been performed. We expect glucose-enhanced MRI will provide a low-risk and cheaper alternative for patients with limited kidney function and a complementary contrast for cancer studies in which contrast enhanced CT and MRI are used for diagnosis and prognosis.

## Acknowledgments

This study was supported by NIH R01EB019934 (NIBIB), P50CA103175 (NCI), R01EB015032 (NIBIB), S10RR028955 (NCRR) and R21EB018934 (NIBIB)

## References

1. O'Connor JP, Tofts PS, Miles KA, Parkes LM, Thompson G, Jackson A. Dynamic contrast-enhanced imaging techniques: CT and MRI. Br J Radiol. 2011; 84(Spec No 2):S112–S120. [PubMed: 22433822]
2. Miles KA. Perfusion CT for the assessment of tumour vascularity: which protocol? Br J Radiol. 2003; 76(Spec No 1):S36–S42. [PubMed: 15456712]
3. Jackson, A.; Buckley, DL.; Parker, GJM., editors. Dynamic Contrast-Enhanced Magnetic Resonance Imaging in Oncology. 2005.
4. McDonald RJ, McDonald JS, Kallmes DF, Jentoft ME, Murray DL, Thielen KR, Williamson EE, Eckel LJ. Intracranial Gadolinium Deposition after Contrast-enhanced MR Imaging. Radiology. 2015; 275(3):772–782. [PubMed: 25742194]
5. Chan KWY, McMahon MT, Kato Y, Liu G, Bulte JWM, Bhujwalla ZM, Artemov D, van Zijl PCM. Natural D-glucose as a biodegradable MRI contrast agent for detecting cancer. Magn Reson Med. 2012; 68(6):1764–1773. [PubMed: 23074027]
6. Walker-Samuel S, Ramasawmy R, Torrealdea F, Rega M, Rajkumar V, Johnson SP, Richardson S, Goncalves M, Parkes HG, Arstad E, Thomas DL, Pedley RB, Lythgoe MF, Golay X. In vivo imaging of glucose uptake and metabolism in tumors. Nat Med. 2013; 19(8):1067–1072. [PubMed: 23832090]
7. Liepinsh E, Otting G. Proton exchange rates from amino acid side chains--implications for image contrast. Magn Reson Med. 1996; 35(1):30–42. [PubMed: 8771020]
8. Ward KM, Aletras AH, Balaban RS. A New Class of Contrast Agents for MRI Based on Proton Chemical Exchange Dependent Saturation Transfer (CEST). J Magn Reson. 2000; 143(1):79–87. [PubMed: 10698648]
9. van Zijl PCM, Jones CK, Ren J, Malloy CR, Sherry AD. MRI detection of glycogen in vivo by using chemical exchange saturation transfer imaging (glycoCEST). Proc Natl Acad Sci U S A. 2007; 104(11):4359–4364. [PubMed: 17360529]
10. Ling W, Regatte RR, Navon G, Jerschow A. Assessment of glycosaminoglycan concentration in vivo by chemical exchange-dependent saturation transfer (gagCEST). Proc Natl Acad Sci U S A. 2008; 105(7):2266–2270. [PubMed: 18268341]
11. Saar G, Zhang B, Ling W, Regatte RR, Navon G, Jerschow A. Assessment of GAG Concentration Changes in the Intervertebral Disc via CEST. Nmr Biomed. 2012; 25(2):255–261. [PubMed: 22253087]
12. McMahon MT, Gilad AA, DeLiso MA, Berman SM, Bulte JW, van Zijl PC. New "multicolor" polypeptide diamagnetic chemical exchange saturation transfer (DIACEST) contrast agents for MRI. Magn Reson Med. 2008; 60(4):803–812. [PubMed: 18816830]
13. Nasrallah FA, Pages G, Kuchel PW, Golay X, Chuang K-H. Imaging brain deoxyglucose uptake and metabolism by glucoCEST MRI. J Cereb Blood Flow Metab. 2013; 33(8):1270–1278. [PubMed: 23673434]
14. Rivlin M, Horev J, Tsarfaty I, Navon G. Molecular imaging of tumors and metastases using chemical exchange saturation transfer (CEST) MRI. Sci Rep. 2013; 3

15. Rivlin M, Tsarfaty I, Navon G. Functional molecular imaging of tumors by chemical exchange saturation transfer MRI of 3-O-Methyl-D-glucose. Magn Reson Med. 2014; 72(5):1375–1380. [PubMed: 25236979]
16. Jin T, Mehrens H, Hendrich KS, Kim S-G. Mapping brain glucose uptake with chemical exchange-sensitive spin-lock magnetic resonance imaging. J Cereb Blood Flow Metab. 2014; 34(8):1402–1410. [PubMed: 24865996]
17. Zu Z, Spear J, Li H, Xu J, Gore JC. Measurement of regional cerebral glucose uptake by magnetic resonance spin-lock imaging. Magn Reson Imaging. 2014; 32(9):1078–1084. [PubMed: 24960367]
18. Yadav NN, Xu J, Bar-Shir A, Qin Q, Chan KWY, Grgac K, Li W, McMahon MT, van Zijl PCM. Natural D-glucose as a biodegradable MRI relaxation agent. Magn Reson Med. 2014; 72(3):823–828. [PubMed: 24975029]
19. Gore JC, Brown MS, Mizumoto CT, Armitage IM. Influence of glycogen on water proton relaxation times. Magn Reson Med. 1986; 3(3):463–466. [PubMed: 3724426]
20. Lal B, Goodwin CR, Sang Y, Foss CA, Cornet K, Muzamil S, Pomper MG, Kim J, Laterra J. EGFRvIII and c-Met pathway inhibitors synergize against PTEN-null/EGFRvIII+ glioblastoma xenografts. Mol Cancer Ther. 2009; 8(7):1751–1760. [PubMed: 19584231]
21. Zhu W, Kato Y, Artemov D. Water exchange-minimizing DCE-MRI protocol to detect changes in tumor vascular parameters: effect of bevacizumab/paclitaxel combination therapy. Magma (New York, NY). 2014; 27(2):161–170.
22. Donahue KM, Weisskoff RM, Chesler DA, Kwong KK, Bogdanov AA Jr, Mandeville JB, Rosen BR. Improving MR quantification of regional blood volume with intravascular T1 contrast agents: accuracy, precision, and water exchange. Magn Reson Med. 1996; 36(6):858–867. [PubMed: 8946351]
23. Puri BK, Lewis HJ, Saeed N, Davey NJ. Volumetric change of the lateral ventricles in the human brain following glucose loading. Experimental physiology. 1999; 84:223–226. [PubMed: 10081720]
24. Mueckler M. Facilitative glucose transporters. Eur J Biochem. 1994; 219(3):713–725. [PubMed: 8112322]
25. Artemov D, Bhujwalla ZM, Pilatus U, Glickson JD. Two-compartment model for determination of glycolytic rates of solid tumors by in vivo 13C NMR spectroscopy. NMR Biomed. 1998; 11(8):395–404. [PubMed: 10221582]
26. Minakami S, Yoshikawa H. thermodynamic Considerations on Erythrocyte Glycolysis. Biochem Biophys Res Commun. 1965; 18:345–349. [PubMed: 14300746]
27. Garrett RH, Grisham CM. Biochemistry. 2010
28. Van Zijl PC, Davis D, Eleff SM, Moonen CT, Parker RJ, Strong JM. Determination of cerebral glucose transport and metabolic kinetics by dynamic MR spectroscopy. Am J Physiol. 1997; 273:E1216–E1227. [PubMed: 9435539]
29. Gruetter R. Glycogen: the forgotten cerebral energy store. J Neurosci Res. 2003; 74(2):179–183. [PubMed: 14515346]
30. Rothman DL, Novotny EJ, Shulman GI, Howseman AM, Petroff OA, Mason G, Nixon T, Hanstock CC, Prichard JW, Shulman RG. 1H-[13C] NMR measurements of [4-13C]glutamate turnover in human brain. Proc Natl Acad Sci U S A. 1992; 89(20):9603–9606. [PubMed: 1409672]
31. Shulman RG, Rothman DL, Behar KL, Prichard JW. High resolution NMR studies of cerebral glucose metabolism in rats and humans. Adv Exp Med Biol. 1991; 291:5–8. [PubMed: 1927690]
32. Tofts PS, Brix G, Buckley DL, Evelhoch JL, Henderson E, Knopp MV, Larsson HBW, Lee T-Y, Mayr NA, Parker GJM, Port RE, Taylor J, Weisskoff RM. Estimating kinetic parameters from dynamic contrast-enhanced t1-weighted MRI of a diffusable tracer: Standardized quantities and symbols. J Magn Reson Imaging. 1999; 10(3):223–232. [PubMed: 10508281]
33. Tofts PS. Modeling tracer kinetics in dynamic Gd-DTPA MR imaging. J Magn Reson Imaging. 1997; 7(1):91–101. [PubMed: 9039598]

34. Gruetter R, Novotny EJ, Boulware SD, Rothman DL, Shulman RG. 1H NMR studies of glucose transport in the human brain. J Cereb Blood Flow Metab. 1996; 16(3):427–438. [PubMed: 8621747]

35. Shestov AA, Emir UE, Kumar A, Henry PG, Seaquist ER, Oz G. Simultaneous measurement of glucose transport and utilization in the human brain. Am J Physiol Endocrinol and Metab. 2011; 301(5):E1040–E1049. [PubMed: 21791622]

36. Zhou J, Payen J-F, Wilson DA, Traystman RJ, van Zijl PCM. Using the amide proton signals of intracellular proteins and peptides to detect pH effects in MRI. Nat Med. 2003; 9(8):1085–1090. [PubMed: 12872167]

37. Kim M, Gillen J, Landman BA, Zhou J, van Zijl PCM. Water saturation shift referencing (WASSR) for chemical exchange saturation transfer (CEST) experiments. Magn Reson Med. 2009; 61(6):1441–1450. [PubMed: 19358232]

38. Sun PZ, Farrar CT, Sorensen AG. Correction for artifacts induced by B0 and B1 field inhomogeneities in pH-sensitive chemical exchange saturation transfer (CEST) imaging. Magn Reson Med. 2007; 58(6):1207–1215. [PubMed: 17969015]

39. Reagan-Shaw S, Nihal M, Ahmad N. Dose translation from animal to human studies revisited. FASEB journal : official publication of the Federation of American Societies for Experimental Biology. 2008; 22(3):659–661. [PubMed: 17942826]

40. Lozner EL, Winkler AW, Taylor FH, Peters JP. The Intravenous Glucose Tolerance Test. J Clin Invest. 1941; 20(5):507–515. [PubMed: 16694855]

41. Xu, X.; Jones, CK.; Yadav, NN.; Knutsson, L.; Hua, J.; Kalyani, R.; Hall, E.; Laterra, J.; Blakeley, J.; Strowd, R.; Ambady, P.; Pomper, M.; Barker, P.; Liu, G.; Chan, KWY.; McMahon, MT.; Stevens, RD.; van Zijl, PCM. Proceedings of the ISMRM. Toronto: 2015. Dynamic Imaging of D-Glucose at 7T: First Experiments in Human Brain; p. 1767

42. Noguchi T, Yoshiura T, Hiwatashi A, Togao O, Yamashita K, Nagao E, Shono T, Mizoguchi M, Nagata S, Sasaki T, Suzuki SO, Iwaki T, Kobayashi K, Mihara F, Honda H. Perfusion imaging of brain tumors using arterial spin-labeling: correlation with histopathologic vascular density. Am J Neuroradiol. 2008; 29(4):688–693. [PubMed: 18184842]

43. Zhou J, Wilson DA, Ulatowski JA, Traystman RJ, van Zijl PC. Two-compartment exchange model for perfusion quantification using arterial spin tagging. J Cereb Blood Flow Metab. 2001; 21(4): 440–455. [PubMed: 11323530]

44. Carruthers A. Facilitated diffusion of glucose. Physiological Reviews. 1990; 70(4):1135–1176. [PubMed: 2217557]

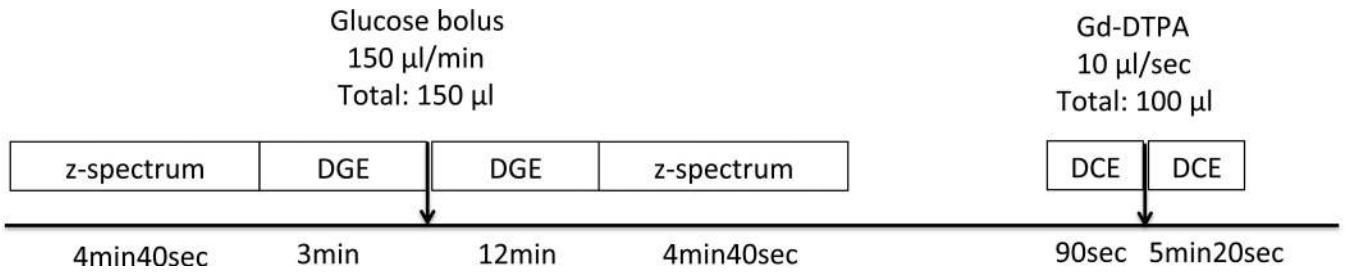


**Figure 1.**

Timing of the dynamic glucose enhanced (DGE) and dynamic contrast enhanced (DCE) acquisition. D-glucose (2.8 M) was injected at 2.5 µl/s while Gd-DTPA (100 mM) was injected at 10 µl/s. DCE images were acquired one hour post glucose injection. Both the glucose and Gd-DTPA bolus were given without stopping the scan or re-positioning the mice.

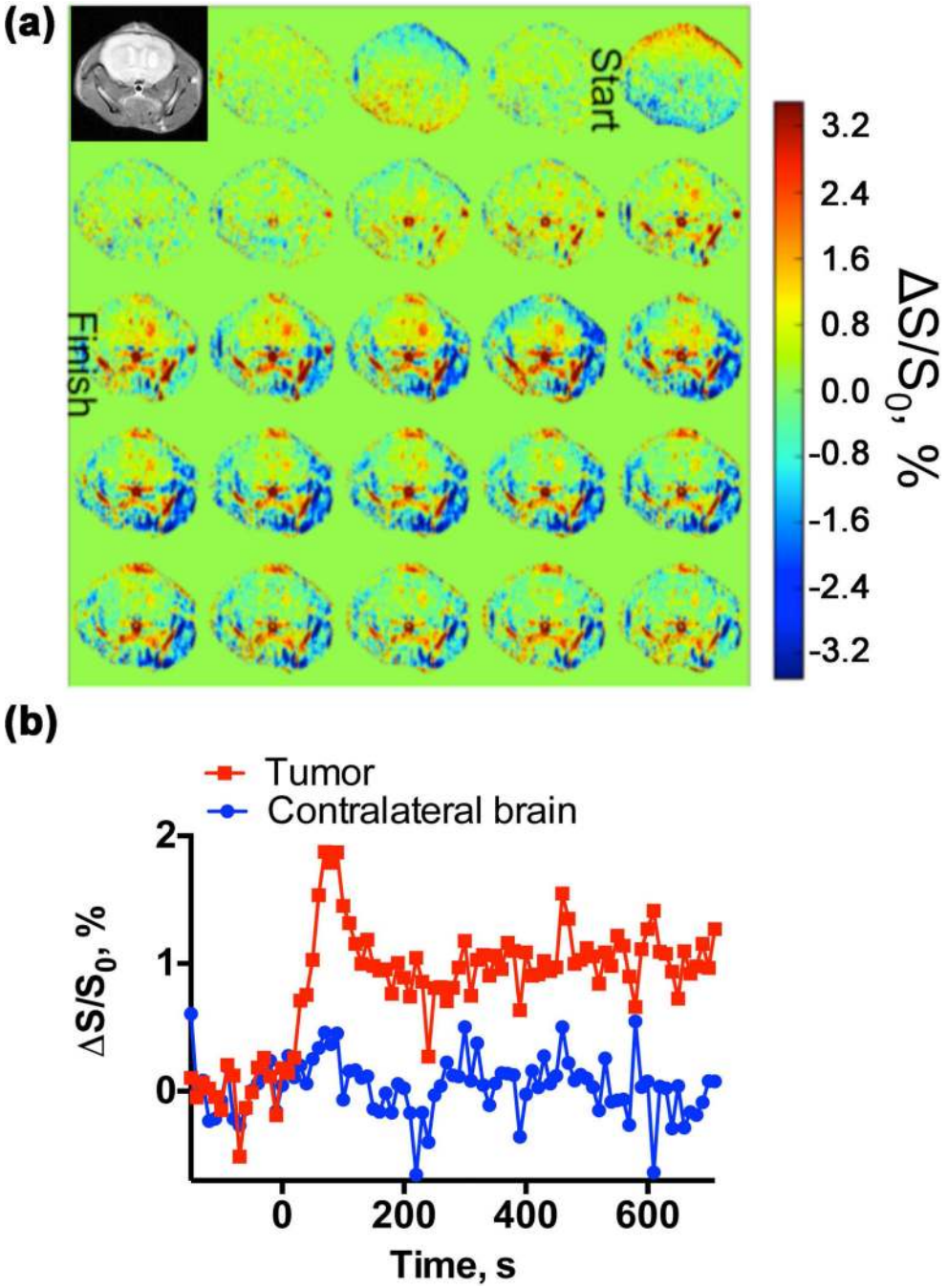


**Figure 2.**

**(a)** Anatomical image and DGE difference images (pre-injection – post-injection, all images acquired at frequency offset of 1.2 ppm) of the head of a representative mouse, showing the highlighting of the vessels and tumor after D-glucose injection. Each image reflects change in 10-s intervals, and the color bar represents the absolute value of the percentage change of the water signal ($\Delta S/S_0$). **(b)** Dynamic time curves for the tumor and contralateral sides of the brain over 12 min.

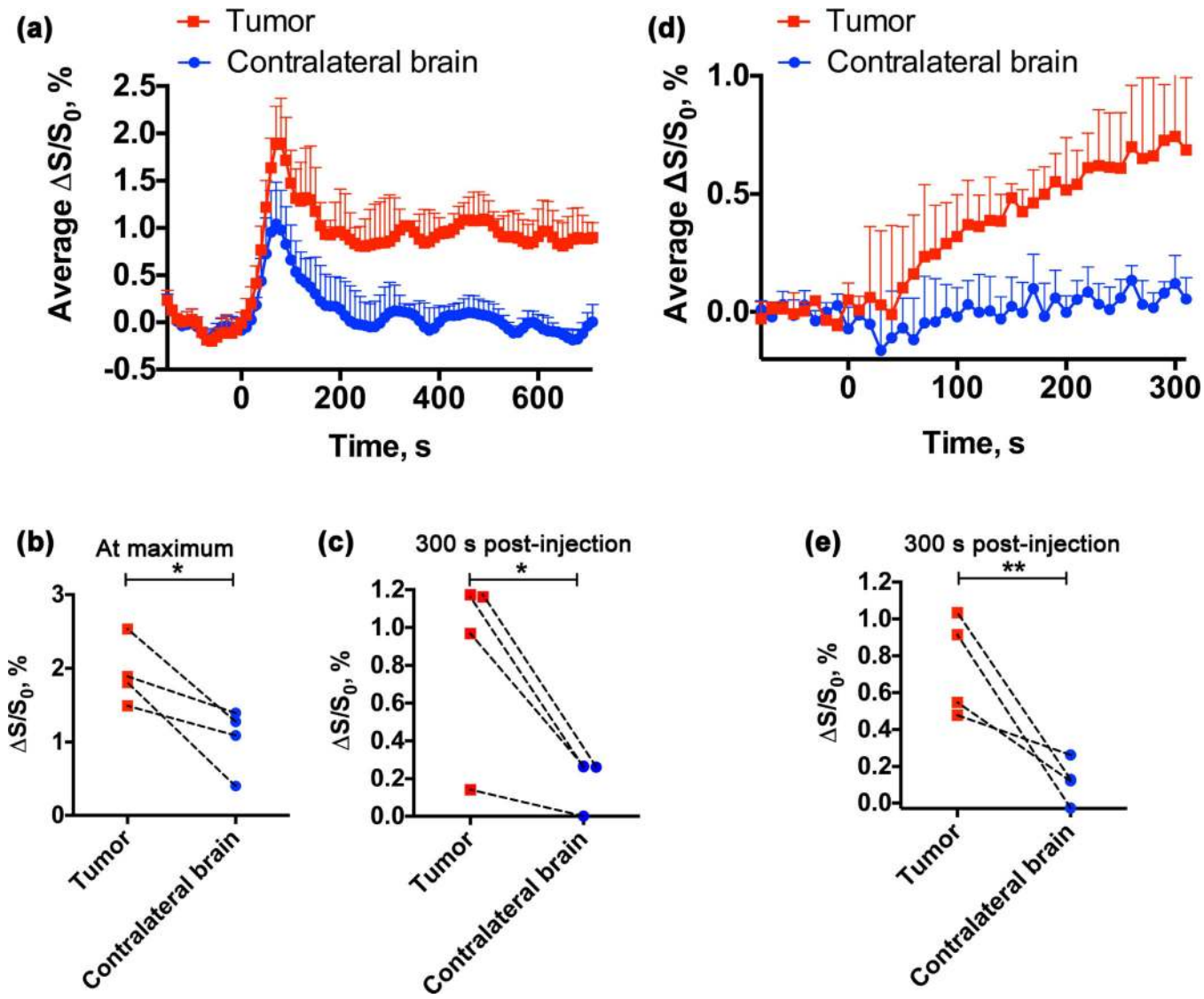


**Figure 3.**

**(a)** Dynamic time curves showing the average (n = 4) glucose difference signal ($\Delta S/S_0$) for the tumor and the contralateral brain. The error bars reflect the standard deviation. The difference between the tumor and the contralateral brain ($\Delta S$) at **(b)** maximal enhancement and **(c)** 300 s post-injection for individual mice indicate a higher uptake in tumor. **(d)** Dynamic time curves showing the average (n = 4) difference in DCE between the tumor and the contralateral brain; **(e)** and at 300 s post-injection for individual mice. (*, $p<0.05$; **, $p<0.01$).

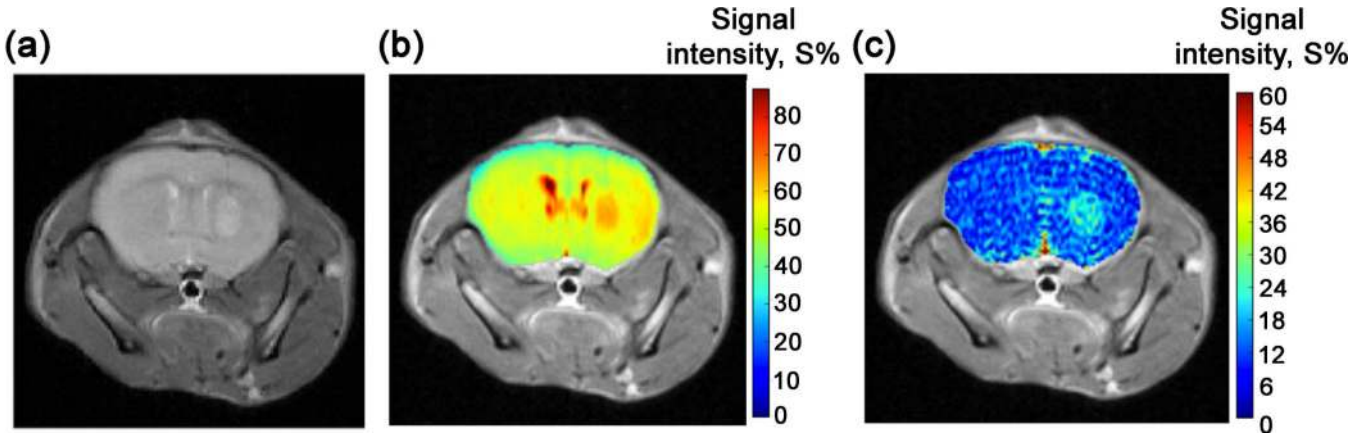


**Figure 4.**

**(a)** Anatomical image for a representative mouse, and the images at 300 s post-injection for DGE **(b)** and DCE **(c)**, respectively, showing the signal intensity (S) of the tumor and the brain.

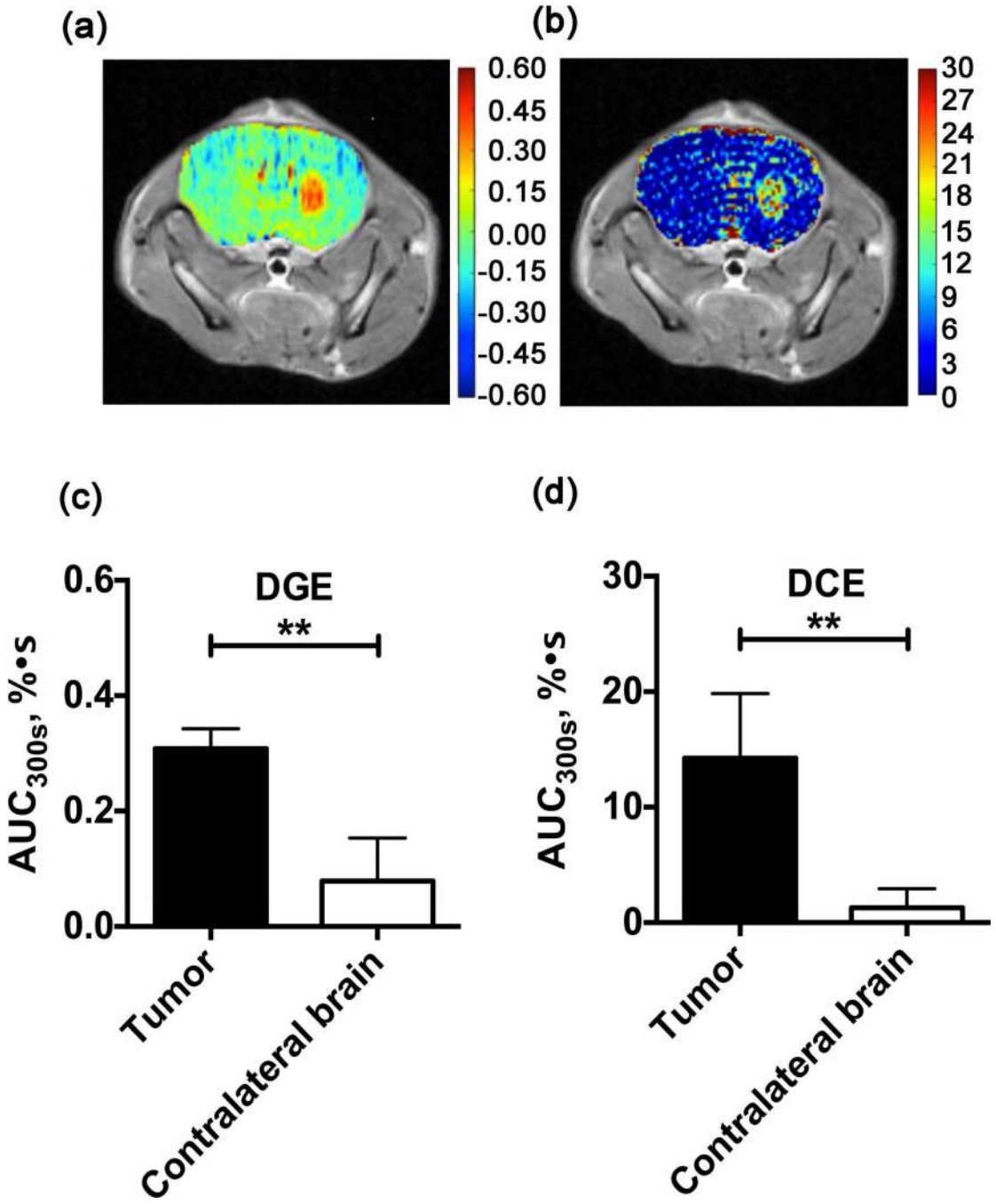


**Figure 5.**

Area-under-curve images over a period of 300 s for **(a)** DGE; **(b)** DCE. **(c)** and **(d)** show the statistics for four mice. Student's t tests, p= 0.001 and 0.004 for DGE and DCE, respectively.

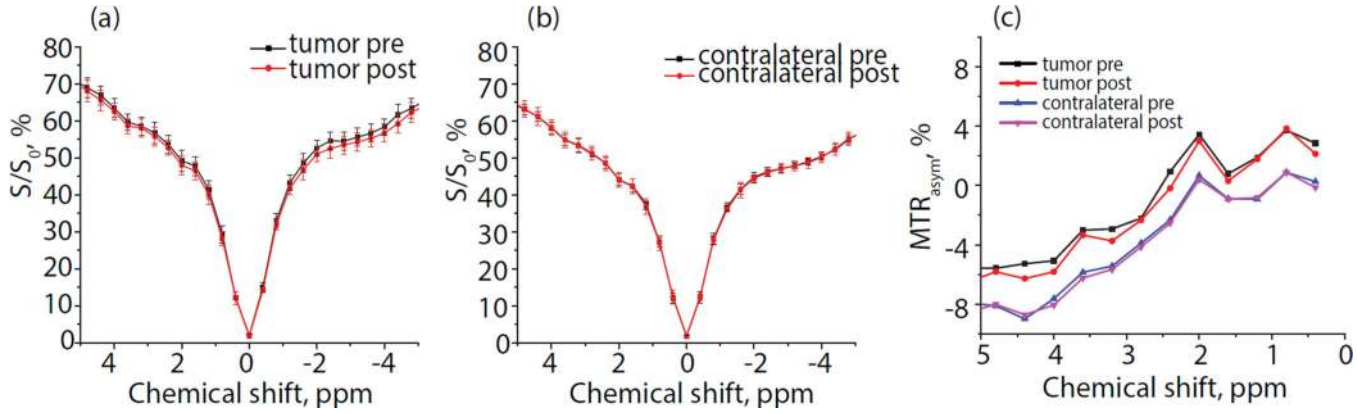


**Figure 6.**

Average Z-spectra (N=4) acquired before and 33 min after glucose injection in **(a)** tumor, **(b)** contralateral brain. **(c)** The corresponding $MTR_{asym}$ spectra.